PHYSICAL REVIEW E **80**, 015303(R) (2009)

# Scaling of the spatial power spectrum of excitations at the onset of solutal convection in a nanofluid far from equilibrium

Fabio Giavazzi* and Alberto Vailati†
*Dipartimento di Fisica and CNISM, Università degli Studi di Milano, via Celoria 16, 20133 Milano, Italy*
(Received 8 April 2009; published 9 July 2009)

We investigate pattern formation in the very early stages of solutal convective instabilities in a suspension of highly thermophilic nanoparticles heated from above. The processing of shadowgraph images allows us to recover the spatial power spectrum of the excitations at the onset. Remarkably, the power spectra obtained at large solutal Rayleigh numbers $2.56\times10^6\leq \mathrm{Ra}_s\leq 4.53\times10^8$ scale onto a single curve without adjustable parameters. The critical wave number exhibits power-law scaling with exponent 1/4 as a function of $\mathrm{Ra}_s$, in excellent agreement with recent theoretical predictions.

DOI: 10.1103/PhysRevE.80.015303 PACS number(s): 47.54.−r, 47.20.Bp, 89.75.Da

The spontaneous formation of patterns occurs in a countless number of natural systems as different as chemical reactions, morphology and decoration of living beings, the appearance of landscape, galaxies, and the crowding of populations, just to mention a few examples [1]. The identification of universal ingredients in the mechanism leading to pattern formation represents an essential step for the formulation of unified models. Within this scenario, convective instabilities in simple liquids and binary mixtures are remarkably relevant as they represent a model system for the understanding of pattern formation in systems driven away from equilibrium [2,3]. The investigation of the onset of the instabilities is of particular importance, because the spontaneous selection of a critical wave number provides the first imprint for the development of the convective pattern. Up to now the investigation of the excitations at the onset has been performed mostly near the threshold of the instability [4]. These studies have clearly shown that the patterns formed at the onset of convection close to threshold are dominated by a single wave number. On the contrary, pattern formation at the onset of convection at high Rayleigh numbers $\mathrm{Ra}=\alpha g\Delta T h^3/(\nu\chi)$ has not been investigated much. Here $\alpha$ is the thermal expansion coefficient, $h$ is the sample thickness, $\nu$ is the kinematic viscosity, $\chi$ is the thermal diffusivity, and $\Delta T$ is the temperature difference. The case of high Ra is of particular relevance in many natural phenomena, such as the convection of heat in the earth mantle, in the atmosphere, and in the oceans. At large Ra the rapid imposition of a temperature gradient is followed by the sudden formation and destabilization of thermal boundary layers (BLs). However, due to the finite thermal conductivity of the thermalizing plates, the time needed to impose the temperature gradient is typically of the same order of that needed for the destabilization of the BLs. This makes difficult to achieve an accurate characterization of the pattern at the onset.

Binary mixtures, in particular suspensions of nanoparticles (nanofluids), represent an ideal system to investigate pattern formation at the onset of the instability at large solutal Rayleigh numbers [5]. In this case by rapidly heating from above a suspension made of highly thermophilic nanoparticles one is able to generate gravitationally unstable concentration BLs leading to a solutal instability. For a nanofluid the buildup of the unstable concentration BLs takes place in a time $10^4$–$10^5$ times larger than that of temperature BLs in a simple fluid. This allows us to achieve an accurate characterization of the unstable excitations at the onset. A first understanding of the onset of the instability can be attained by investigating the transient relaxation oscillations of the convective flow [6–11]. A more challenging and refined understanding of pattern formation involves the investigation of the power spectrum of the excitations of the BLs at the onset. Such spectrum is difficult to predict from theoretical models and simulations, which instead rely on assumptions on the spatial spectral properties of the system (typically a single mode). Therefore, beyond its general importance for the understanding of pattern formation in nonequilibrium systems, the determination of the spectrum is of great relevance to provide a solid foundation for the development of meaningful models and simulations.

In this work we use a sensitive quantitative shadowgraph technique to determine the power spectrum of the excitations at the onset of a solutal convective instability at large solutal Rayleigh numbers. The processing of the spatial power spectrum of the shadowgraph images of excitations at the onset shows unambiguously the presence of a dominant critical wave number $\kappa^*$. The scaling of $\kappa^*$ with the solutal Rayleigh number $\mathrm{Ra}_s=\beta g c(1-c)S_T\Delta T h^3/(\nu D)$ is compatible with a power law with exponent of 1/4, in agreement with recent theoretical models [9,12–14]. Here $\beta=\rho^{-1}\partial\rho/\partial c$ is the solutal expansion coefficient, $S_T$ is the Soret coefficient, $c$ is the weight fraction concentration of nanoparticles, and $D$ is the diffusion coefficient. The bandwidth of the excited modes is of the order of $\Delta\kappa^*\simeq\kappa^*/3$, irrespective of the value of $\mathrm{Ra}_s$. Quite remarkably, we find that the spatial power spectra of the excitations at the onset can be rescaled onto a single master curve without any adjustable parameter.

The solutal instability is induced by imposing a temperature difference to a horizontal layer of a nanofluid made of highly thermophilic nanoparticles. The thermophilic nature of the particles gives rapidly rise to the accumulation (deple-

*Present address: Dipartimento di Chimica, Biochimica e Biotecnologie per la Medicina, Università degli Studi di Milano, via F. Cervi 93, 20090 Segrate (Milano), Italy; fabio.giavazzi@unimi.it
†alberto.vailati@unimi.it

 

tion) of nanoparticles near the upper (bottom) plate, thus creating two thin concentration BLs. The BLs grow diffusively and when they reach a critical thickness they become gravitationally unstable and convection sets in [8]. The nanofluid is heated from above so that it is stable against Rayleigh-Bénard convection and a linear conductive temperature profile develops inside it. The thermal dilation of the fluid gives rise to a stable density gradient $\nabla\rho_T=\rho\alpha\nabla T$. The temperature difference induces a mass flow through the Soret effect [15]. Close to the BLs the mass flow creates a nonequilibrium concentration gradient $\nabla c=S_T c(1-c)\nabla T$ and in turn a density gradient $\nabla\rho_s=\rho\beta\nabla c$. In the case of a nanofluid, both the thermal dilation and the concentration of the particles contribute to the nonequilibrium density profile. The relative weight of the two contributions is represented by the separation ratio $\Psi=\nabla\rho_s/\nabla\rho_T=\beta S_T c(1-c)/\alpha$. The control parameter for the onset of the instability is the solutal Rayleigh number $\mathrm{Ra}_s$ [16]. The threshold condition for the onset of a solutal instability in the presence of no-slip impermeable boundaries is $\mathrm{Ra}_s>720$ [17].

The sample is a dilute aqueous suspension of spherical silica nanoparticles with a diameter of 32 nm (Ludox©TMA). At the working concentration (weight fraction $c=4.1\%$) it has a large negative separation ratio $\Psi=-3.41$. Another key feature is its very low Lewis number $\mathrm{Le}=D/\chi\simeq 10^{-4}$, which provides the order of magnitude of the ratio between the characteristic time scales associated with the development of thermal and concentration BLs [18]. The experimental setup has been described in detail elsewhere [7]. The sample is confined in a cylindrical Rayleigh-Bénard cell of variable diameter $d$ (38 and 47 mm) and thickness (1, 1.3, 2, and 2.9 mm). The corresponding aspect ratio spans the range $16\leq\phi/h\leq 38$. The sample is sandwiched between two horizontal sapphire windows whose temperature are maintained by two annular thermoelectric devices independently controlled by proportional integral servo controls. The time needed for reaching 64% of set point temperature difference between the plates starting from an isothermal condition is about 35 s. The sample is imaged by means of a shadowgraph setup [19]. A collimated quasimonochromatic beam (central wavelength $\lambda=675$ nm and spectral bandwidth $\Delta\lambda=13$ nm) is sent onto the sample, the optical axis being orthogonal to the confining plates. A lens collects the light emerging from the sample and conjugates a plane at a distance $z$ from the cell with the plane of a charge coupled device (CCD) sensor.

Each measurement starts with the sudden imposition at $t=0$ of a temperature difference $\Delta T$ to the plates confining the initially isothermal sample at $T_0=30\ ^\circ\mathrm{C}$, the set-point temperatures of the upper and the lower plate being $T_0+\Delta T/2$ and $T_0-\Delta T/2$, respectively. The investigated range of $\Delta T$ is 6–32 K. At $t=0$ the acquisition of the shadowgraph images is started, at the rate of one image every 5 s. An image $I_0(x,y)$ accounting for the illumination inhomogeneities is obtained by averaging the first $N=40$ shadowgraph images acquired well before the observed onset of convection. The shadowgraph signal $S^{(i)}(x,y)=[I^{(i)}(x,y)-I_0(x,y)]/I_0(x,y)$ associated to each image $I^{(i)}(x,y)$ is then extracted. Here $x$ and $y$ indicate the coordinates of a pixel and $i$ labels the images in the sequence. From an optical point of view, the sample is modeled as a thin transparent slab. Its refractive index $n(x,y,z)=n_0+n'(x,y,z)$ is the superposition of an average term $n_0$, slightly perturbed by the term $n'=\partial n/\partial c\Delta c$ due to concentration inhomogeneities $\Delta c$ induced in the fluid by the solutal convective motions. Under the assumption that refractive index fluctuations are small the power spectrum of the shadowgraph signal $\Phi(\mathbf{k})=|\hat{S}(\mathbf{k})|^2$ is given by $\Phi(\mathbf{k})=H(\mathbf{k})|\hat{\phi}(\mathbf{k})|^2$, where $\phi(x,y)=k_0\int dz n'(x,y,z)$ is the phase delay introduced by the sample in the incoming wave and $H$ is the shadowgraph transfer function [20]. Here $k_0=2\pi/\lambda$, the symbol $\hat{}$ denotes the two-dimensional Fourier transform, and $\mathbf{k}=(k_x,k_y)$. To perform our measurements we have chosen to use a suitably small value of $z=3.0$ cm so that in the wave number range investigated by us the transfer function can be approximated by the power law $H(\mathbf{k})\simeq[zk^2/k_0]^2$ [21]. An estimate of the spectrum $\Phi_B(\mathbf{k})$ of the background noise is obtained by averaging the power spectra of the first $N$ shadowgraph images so to get rid of the noise generated by the detection chain. A reliable indicator of the overall strength of the convective motion inside the sample is recognized to be the variance $\sigma_i^2=\frac{1}{M}\Sigma_{x,y}[S^{(i)}(x,y)]^2$ of the shadowgraph signal, which is strictly related to the total power of the horizontal concentration fluctuations inside the sample [8]. Here $M$ is the total number of pixels in one image. After the imposition of the temperature difference, $\sigma_i^2$ remains stable for a long time. After this latency time the amplitude of the signal suddenly grows up to a peak, followed by a set of damped oscillations leading to a steady state [7,8]. The steady state is characterized by a multimodal spoke pattern [22,23]. We identify the onset of the instability with the instant when $\sigma_i^2$ exceeds for the first time its mean value by more than three times its standard deviation. The mean value and the standard deviation of $\sigma_i^2$ in this initial phase are estimated on the base of the first $N$ images taken during the latency time preceding the onset. Actually, the rise of $\sigma_i^2$ is very sharp and monotone and this allows an unambiguous determination of the onset [8].

The results discussed in this Rapid Communication refer to the early stages of pattern formation when the convective excitations of the BLs become barely detectable. Figure 1(a) shows a sample shadowgraph image of the excitations at the onset of the instability at $\mathrm{Ra}_s=4.26\times 10^6$. Figure 1(b) shows the two-dimensional power spectrum $\Phi(\mathbf{k})-\Phi_B(\mathbf{k})$ of the shadowgraph signal of Fig. 1(a). The annulus in Fig. 2(b) clearly shows the presence of a characteristic wave number at $k\approx 1.3\times 10^4\ \mathrm{m}^{-1}$. The spectrum is then divided by the transfer function to obtain the spectral distribution of the excitations inside the sample $\Phi^*(\mathbf{k})=[\Phi(\mathbf{k})-\Phi_B(\mathbf{k})]/H(\mathbf{k})$. $\Phi^*$ is proportional to the power spectrum of the vertically averaged fluctuations of the concentration field around its mean value. The azimuthal average $P(k)$ of $\Phi^*(\mathbf{k})$, shown in Fig. 1(c), exhibits a single fairly symmetric peak at $k^*\approx 1.2\times 10^4\ \mathrm{m}^{-1}$. In order to obtain an estimate of the dominant wave number and of the characteristic spectral width, we fitted the spectral profile with a Gaussian function of the form $G(\kappa)=A\exp[-(\kappa-\kappa^*)^2/(2\Delta\kappa^2)]$, where $\kappa^*=hk^*$ and $\Delta\kappa^*=h\Delta k^*$ represent the dimensionless peak position

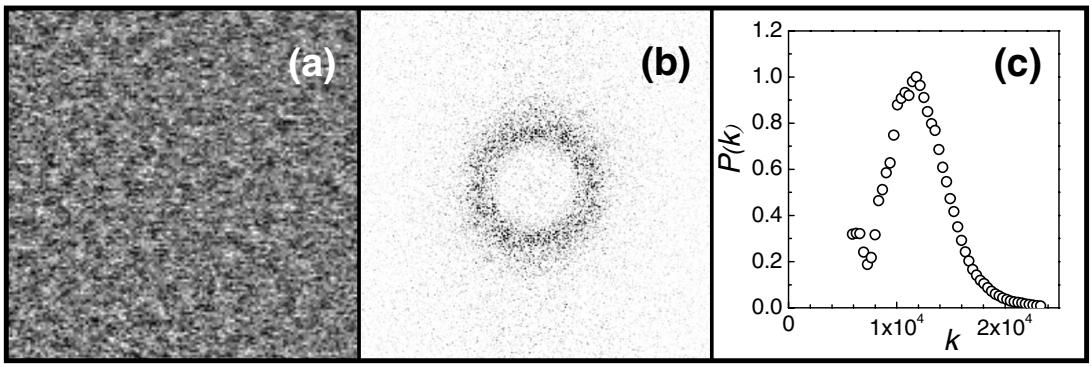


FIG. 1. (a) Shadowgraph image of the excitations at the onset of solutal convection at $\mathrm{Ra}_s = 4.26 \times 10^6$. The side of the image is 5mm. The contrast of the image has been greatly enhanced to make the barely detectable excitations at the onset apparent. (b) Power spectrum of the image in panel (a). One can appreciate the rotational symmetry of the spectrum and the presence of a characteristic wave number $k \approx 1.3 \times 10^4$ m$^{-1}$. The side of the image corresponds to $9 \times 10^4$ m$^{-1}$. (c) Azimuthally averaged power spectrum of the data in panel (b) corrected by diving by the shadowgraph transfer function. The noise at small wave numbers is due to the small sensitivity of shadowgraph in this region.

and width, respectively. The observed dependence of $\kappa^*$ and $\Delta\kappa^*$ from the solutal Rayleigh number $\mathrm{Ra}_s$ is reported in Fig. 2. Both $\kappa^*$ and $\Delta\kappa^*$ clearly exhibit a power-law dependence from $\mathrm{Ra}_s$. The fitting of the data points yields $\kappa^* = (0.3 \pm 0.1)\mathrm{Ra}_s^{0.24 \pm 0.02}$ and $\Delta\kappa^* = (0.10 \pm 0.05)\mathrm{Ra}_s^{0.25 \pm 0.02}$. The scaling exponent of $\kappa^*$ is fully consistent with the value of 1/4, recently predicted theoretically with different methods [9,12,14]. In particular, the scaling of $\kappa^*$ is in excellent agreement with the theoretical predictions by Kim *et al.* [12] for $\mathrm{Le} \to 0$, represented by the continuous line in Fig. 2. Moreover, the prefactor $0.3 \pm 0.1$ found by us for the scaling of $\kappa^*$ is fully compatible with the value 0.2585 predicted by Kim *et al.* A result which has not yet a theoretical counterpart is that the bandwidth $\Delta\kappa^*$ of the excited wave numbers is observed to scale with $\mathrm{Ra}_s$ exactly as $\kappa^*$ does. This strongly suggests that the scaling at the onset involves the entire spectrum of excitations. The inset of Fig. 3 shows the azimuthally averaged spectrum $P(\kappa)/P_p$ at the onset of convection plotted as a function of $\kappa$ at different $\mathrm{Ra}_s$. The amplitude of each curve has been normalized to its peak value $P_p$. The main panel Fig. 3 shows the same curves rescaled along the $\kappa$ axis by adopting $\kappa^*$ as a unit wave number. One can immediately appreciate the nice collapse of the curves onto a single curve with the exception of small wave numbers where the small sensitivity of shadowgraph does not allow us to take reliable measurements. We would like to emphasize that the scaling is obtained without adjustable parameters, the scaling factor $\kappa^*$ being calculated for each curve from the solutal Rayleigh number alone by using the experimental scaling relation $\kappa^* = 0.3\mathrm{Ra}_s^{0.24}$.

In conclusion, we have investigated pattern formation at

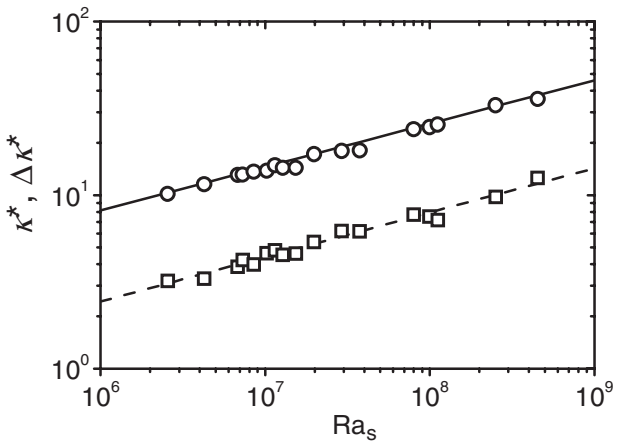


FIG. 2. Dominant wave number $\kappa^*$ (circles) and spectral bandwidth $\Delta\kappa^*$ (squares) at the onset of the instability plotted as functions of the solutal Rayleigh number $\mathrm{Ra}_s$. The solid line represents the theoretical prediction by Kim *et al.* $\kappa^* = 0.2585\mathrm{Ra}_s^{0.25}$ [12]. The dashed line is the best fit of $\Delta\kappa^*$ with a power law.

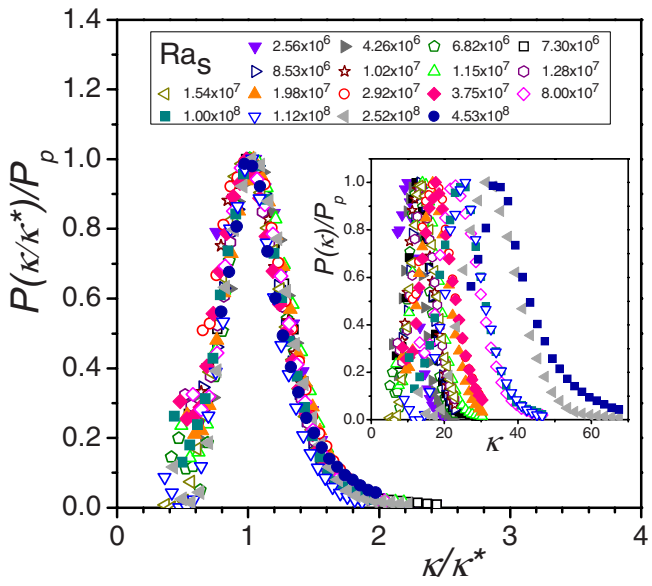


FIG. 3. (Color online) The inset shows the azimuthal average $P(\kappa)/P_p$ of the spectra of the excitations at the onset of convection as a function of the dimensionless wave number $\kappa$. Different curves corresponds to solutal Rayleigh numbers in the range $2.56 \times 10^6 \leq \mathrm{Ra}_s \leq 4.53 \times 10^8$. The main panel shows the same curves plotted as a function of $\kappa/\kappa^*$, where $\kappa^*$ is calculated from the experimental power-law scaling $\kappa^* = 0.3\mathrm{Ra}_s^{0.24}$. The curves have been normalized by dividing them by their peak value.

the onset of a convective instability in a nanofluid at large solutal Rayleigh numbers $Ra_s$. We have shown that the critical wave number scales as a power law of $Ra_s$, with a power-law exponent compatible with 1/4, in excellent agreement with the predictions of recent theoretical models. Quite strikingly, all the relevant length scales of the emerging convective plan form obey to a single scaling law as a function of $Ra_s$, and the power spectra of the excitations at the onset obtained at different $Ra_s$ can be scaled onto a single master curve without adjustable parameters. We feel that this result will provide a reliable and firm reference point for the development of theoretical models and simulations of pattern formation in nonequilibrium systems far from threshold.

We thank M. Giglio for seminal discussion and support to this work. We thank R. Cerbino and S. Mazzoni for stimulating discussion. This work was partially supported by the Italian Ministry for University and Research (MIUR).

[1] P. Ball, *The Self-made Tapestry: Pattern Formation in Nature* (Oxford University, New York, 2001).
[2] M. C. Cross and P. C. Hohenberg, Rev. Mod. Phys. **65**, 851 (1993).
[3] J. P. Gollub and J. S. Langer, Rev. Mod. Phys. **71**, S396 (1999).
[4] See, for example, J. Oh, J. M. Ortiz de Zarate, J. V. Sengers, and G. Ahlers, Phys. Rev. E **69**, 021106 (2004) and references therein.
[5] See, for example, B. Huke, H. Pleiner, and M. Lücke, Phys. Rev. E **75**, 036203 (2007) and references therein.
[6] R. Cerbino, A. Vailati, and M. Giglio, Phys. Rev. E **66**, 055301(R) (2002).
[7] S. Mazzoni, R. Cerbino, D. Brogioli, A. Vailati, and M. Giglio, Eur. Phys. J. E **15**, 305 (2004).
[8] R. Cerbino, S. Mazzoni, A. Vailati, and M. Giglio, Phys. Rev. Lett. **94**, 064501 (2005).
[9] A. Ryskin and H. Pleiner, Phys. Rev. E **71**, 056303 (2005).
[10] V. M. Shevtsova, D. E. Melnikov, and J. C. Legros, Phys. Rev. E **73**, 047302 (2006).
[11] R. Savino and D. Paterna, Phys. Fluids **20**, 017101 (2008).
[12] M. C. Kim, C. K. Choi, and J. K. Yeo, Phys. Fluids **19**, 084103 (2007).
[13] M. C. Kim and C. K. Choi, Phys. Rev. E **76**, 036302 (2007).
[14] See EPAPS Document No. E-PLEEE8-80-R07907 for a simple heuristic derivation of the power-law exponent of 1/4 based on dimensional analysis. For more information on EPAPS see http://www.aip.org/pubservs/epaps.html.
[15] T. E. Faber, *Fluid Dynamics for Physicists* (Cambridge University, Cambridge, England, 1995).
[16] In principle the parameter that mirrors the Rayleigh number in a simple fluid is the modified solutal Rayleigh number $Ra_s\delta$ [8].
[17] J. M. Ortiz de Zarate and J. V. Sengers, *Hydrodynamic Fluctuations* (Elsevier, Amsterdam, 2006).
[18] Other physical properties of the sample are $S_T=-0.047\ K^{-1}$, $D=2.2\times10^{-7}\ cm^2/s$, $\chi=1.48\times10^{-3}\ cm^2/s$, $\alpha=3.03\times10^{-3}\ K^{-1}$, $\nu=8.18\times10^{-3}\ cm^2/s$, and $\beta=0.57$.
[19] G. S. Settles, *Schlieren and Shadowgraph Techniques: Visualizing Phenomena in Transparent Media* (Springer, Berlin, 2001).
[20] S. P. Trainoff and D. S. Cannell, Phys. Fluids **14**, 1340 (2002).
[21] The absence of oscillations in the spectra of shadowgraph images of excitations at the onset [Fig. 1(b)] shows that the power of the excitations is confined at small wave numbers. Therefore, we have restricted our measurement to $k\leq0.75k_m$, a region where the power-law approximation of $H(\mathbf{k})$ is justified. Here $k_m=3.12\times10^4\ m^{-1}$ corresponds to the first peak of $H(\mathbf{k})$ [20].
[22] F. H. Busse, Acta Mech. (Suppl.) **4**, 11 (1994).
[23] S. Mazzoni, F. Giavazzi, R. Cerbino, M. Giglio, and A. Vailati, Phys. Rev. Lett. **100**, 188104 (2008).